

Available online at [www.sciencedirect.com](http://www.sciencedirect.com)

ScienceDirect

Procedia CIRP 31 (2015) 100 – 105

[www.elsevier.com/locate/procedia](http://www.elsevier.com/locate/procedia)

15th CIRP Conference on Modelling of Machining Operations

# An elastoplastic constitutive damage model to simulate the chip formation process and workpiece subsurface defects when machining CFRP composites

S. Zenia<sup>a</sup>, L. Ben Ayed<sup>a</sup>, M. Nouari<sup>a,\*</sup>, A. Delamézière<sup>a</sup>

<sup>a</sup>Laboratoire d'Energétique et de Mécanique Théorique et Appliquée, LEMTA CNRS-UMR 7563, Ecole des Mines d'Albi, Université de Lorraine, GIP-InSIC, 27 rue d'Hellieule, 88100, Saint-Dié-des-Vosges, France

\* Corresponding author. Tel.: +33 3 29 42 22 26; fax: +33 3 29 42 18 25. E-mail address: [mohammed.nouari@mines-nancy.univ-lorraine.fr](mailto:mohammed.nouari@mines-nancy.univ-lorraine.fr)

## Abstract

The machining process of multi-layer composites made of Carbon Fiber Reinforced Polymer (CFRP) generates mainly four damage modes in the workpiece: matrix cracking, debonding at the fiber-matrix interface, fiber rupture and interlaminar delamination. The damage modes mentioned above have been predicted through a user routine "VUMAT", which provides the ability to implement, in Abaqus/Explicit, a combined elastoplastic damage behavior law for progressive failure. The proposed approach is primarily focused on the understanding of interactions between the fiber orientation and the physical phenomena governing the chip formation and the induced damage process.

© 2015 The Authors. Published by Elsevier B.V. This is an open access article under the CC BY-NC-ND license

(<http://creativecommons.org/licenses/by-nc-nd/4.0/>).

Peer-review under responsibility of the International Scientific Committee of the "15th Conference on Modelling of Machining Operations

Keywords: Machining; CFRP composite; Chip formation; Damage

## Nomenclature

### Mechanical parameters

$E_i^0$	Initial elastic modulus of in the $i$ direction [MPa]
$\nu_{12}^0$	Poisson's ratio in the $i$ - $j$ plane
$G_{ij}^0$	Initial shear modulus of a ply in the $i$ - $j$ plan [MPa]
$\rho$	Density [ $\text{kg}/\text{m}^3$ ]
$R_0$	Initial yield stress [MPa]
$a, b$	Hardening parameters
$c$	Coupling parameters

### Damage quantities

$e_0$	Strain energy density of a ply
$D_{ij}$	Variable, $ij$ , of damage
$Y_{ij}$	Thermodynamic forces associated with $d_{ij}$
$b_i$	Coupling terms between the transverse and shear damage
$t_c$	Characteristic time [ $\mu\text{s}$ ]
$G_i$	$G$ is the fracture energy in the $i$ direction [ $\text{N}/\text{mm}^3$ ]
$K_i$	Interface stiffness in the $i$ direction [ $\text{N}/\text{mm}^3$ ]
$t_i$	Stress in the $i$ direction [MPa]
$\eta$	Benzeggagh-Kenan parameter

### Cutting parameters

$F_c$	Cutting force component [N]
$F_t$	Thrust force component [N]

## 1. Introduction

The machinability of composite materials is more difficult compared to the conventional metals and their alloys. That is why the development of knowledge on the behavior of composites is considered as a challenging task to manufacturing engineers. Several works, experimental [1-3] and numerical [4-7], concluded that the fiber orientation is the most important parameter which controls the initiation/progression of the damage and the cutting forces during machining of CFRP composites. However, the optimization of one or several parameters using only experimental approaches often requires expensive trials. So, numerical simulation can be very helpful to find the optimal field of cutting parameters.

Modelling the machining process of composites was firstly investigated by Arola and Ramulu [4]. These authors

presented a finite element model with a predefined fracture plane to simulate the chip formation in the orthogonal cutting operation. They explained the mechanism of the chip formation which is composed into primary and secondary rupture. Other works are also interested in the mechanisms of chip-formation process, cutting forces, induced damage, and surface roughness [5-10].

Different models have been proposed in the field of FRP composites. A quasi-static approach based on a micro-mechanical model was proposed by Gopala Rao et al. [5] to estimate the cutting forces during machining of unidirectional composites. Lasri et al. [6] and Soldani et al. [7] adopted a macroscopic model where the workpiece is modelled as a homogeneous equivalent material (HEM). Zenia et al. [8] proposed a mesomechanical damage model to simulate the chip formation process and predict the machining forces during an orthogonal cutting operation of UD-CFRP composites. In the current investigation, the previous model [8] has been extended to 3D cases, where it is necessary to take into account the interlaminar delamination.

This approach combine the stiffness degradation technique, the effective stress concept and the thermodynamic forces to predict the damage initiation and progression during the chip formation process. The delamination which can occur at the interply interface was also taken into account by using the Cohesive Zone Elements (CZE) procedure available in Abaqus/Explicit package [11]. In this work, the workpiece is modelled as a homogeneous equivalent material (HEM). The model allows a better understanding of the physical phenomena observed during the cutting operation, and gives an accurate numerical tool to simulate the real chip formation, cutting forces, and induced subsurface damage. The obtained numerical results were compared to experiments taken from literature and performed by Iliescu et al. [9] and Phadnis et al. [10]. The comparison shows a good agreement.

## 2. Numerical model

The machining FE model developed in this work is composed of a HEM for the workpiece with a damaged-elastoplastic behavior law, and a rigid body for the cutting tool. The numerical simulations were carried out using two models 2D and 3D for orthogonal cutting and drilling operations, respectively.

### 2.1. Cutting parameters and boundary conditions

Geometry and boundary conditions are shown in Fig.1. The values of cutting parameters and tool dimensions are chosen as those defined in [9] and [10] in order to validate predicted numerical results. Regarding the orthogonal cutting operation (Fig. 1(a)) the rake angle  $\alpha$  is stated equal to  $0^\circ$ , the clearance angle  $\gamma$  is fixed at  $11^\circ$ , the tool edge radius  $r_e$  is equal to  $15 \mu\text{m}$ , the depth of cut  $a_p = 0.2 \text{ mm}$ . The cutting speed  $V_c$  is about  $60 \text{ m/min}$ .

For the drilling operation, the tool geometry and the boundary conditions are shown in Fig. 1(b). The workpiece is laid on a rigid support. The values of the machining parameters are selected from the work of Phadnis et al. [10] in

order to validate the results obtained by simulation with the experimental work. The tool is a twist drill with a 3 mm of diameter, the point angle is taken equal to  $120^\circ$  and the clearance angle  $\gamma = 30^\circ$ . The feed rate is equal to  $150 \text{ m/min}$ ,  $300 \text{ m/min}$  and  $500 \text{ m/min}$  and the spindle speed is equal to  $2500 \text{ rpm}$ .

The tool is modelled as a rigid body and controlled by a reference point where the cutting speed is applied and the machining forces are measured as reaction forces in output. The properties of a CFRP ply of the T300/914 composite are taken from the work of Iliescu et al. [9] and remembered in Table 1. The workpiece is considered as a HEM with a longitudinal modulus in the fiber direction more than ten times higher than the transverse modulus.

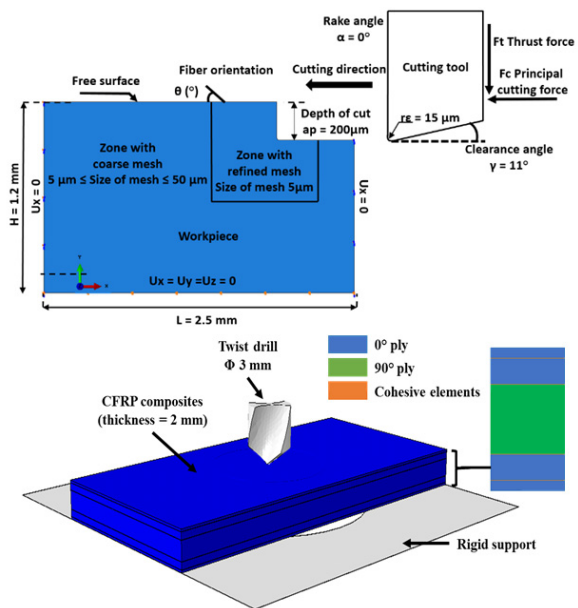


Fig. 1. Boundary condition and geometry of the tool-workpiece couple.

A 3D model is conducted using eight-node linear brick elements with reduced integration, C3D8R available within Abaqus/Explicit.

Table 1. Mechanical properties of CFRP composite T300/914.

Mechanical properties			
$E_1^0$ (MPa)	136600	$\nu_{12}^0$	0.29
$E_2^0$ (MPa)	9600	$\rho$ (kg/m <sup>3</sup> )	1578
$G_{12}^0$ (MPa)	5200		

The near zone of the tool tip where the chip will be formed was finely meshed. In a previous work, Santiuste et al. [7] proved that when the element size is less than or equal to  $7 \mu\text{m}$ , the differences in numerical results is negligible. For the orthogonal cutting operation, the size of elements in this zone is taken about  $5 \mu\text{m}$ . While the remaining part is meshed coarsely with an element size in the range of  $5 \mu\text{m}$  in the vicinity of the finely meshed area and  $50 \mu\text{m}$  on the edges of the workpiece. In the case of drilling operation the element size of the near zone is taken about  $150 \mu\text{m}$  and  $1 \text{ mm}$  on the edges.

A VUMAT subroutine, providing a very general capability for implementing elastoplastic damage models, is used in Abaqus/Explicit. To represent the process of chip formation, based on initiation and damage evolution in the workpiece, the element deletion approach is applied. The interaction between the node set of the workpiece and the tool surface is modeled using surface-to-node contact formulation coupled to kinematic predictor/corrector contact algorithm with finite sliding approach which are available in Abaqus/Explicit package. This methodology allows to have a better simulation of the contact between the tool and the workpiece and this in spite the use of the "element deletion" option that eliminate the most damaged elements. The set of the plastic-damage model parameters reported by Feld [12] have been adopted for the simulations in this work (Table 2).

Table 2. Plastic and damage parameters of UD-CFRP T300/914.

Damage parameters	Plastic parameters		
$Y_{12}^c$ (MPa)	8	$a$	0.54
$Y_{12}^o$ (MPa)	0.03	$b$ (MPa)	1000
$b_1$	0.5	$c$	0.7
$b_2$	0.8	$R_0$ (MPa)	64
$Y_{11}^t$ (MPa)	15		
$Y_{11}^c$ (MPa)	12		
$a$	1		
$t_c$ ( $\mu$ s)	6		

The contact between the tool and the workpiece is done at two contact zones. The first is located between the cutting face and the produced chip. The second is located between the flank face and the machined surface. The interaction between these surfaces (tool/workpiece) is controlled by the Coulomb friction law and the friction coefficient,  $\mu$ , is assumed to be constant during the cutting process (no wear of the cutting tool), as in various numerical studies performed by Gopala et al. [5] and Lasri et al. [6]. In the present study, a coefficient of friction equal to 0.4 was used.

The interply interface was modelled with cohesive elements of type COH3D8 with a thickness of 5  $\mu$ m. According to the literature, different values were used. To simulate the interface degradation, Phadnis et al. [10] and Shin et al. [13] used a thickness of 10 and 5  $\mu$ m, respectively. In our work, the thickness was chosen equal to these used by Shin et al. [13]. However, the use of cohesive elements with a thickness of 5  $\mu$ m or 10  $\mu$ m has no effect on the behavior of the interface.

Table 3. Material parameters used to model interface cohesive elements

Damage parameters			
$K_n$ (N/mm <sup>3</sup> )	$4 \times 10^6$	$t_n^0$ (MPa)	60
$K_s = K_t$ (N/mm <sup>3</sup> )	$4 \times 10^6$	$t_t^0 = t_s^0$ (MPa)	90
$G_n$ (N/mm <sup>3</sup> )	0.2	$\eta$	1.8
$G_s = G_t$ (N/mm <sup>3</sup> )	1		

These cohesive elements are controlled by damage criteria discussed in Section 2.3. The removal of the element is performed, once the degradation parameters reaches the limit value of 0.99 and the failed cohesive elements were removed from the FE model. Mechanical properties of Cohesive Zone

are reported by Phadnis et al. [10] and Shin et al. [13] (Table 3).

## 2.2. Material behavior during machining process: Combined elastoplastic damage law and interface delamination

Here it will be developed that the 3D, concerning the 2D model please refer to the publication of Zenia et al. [8].

### 2.2.1. Progressive damage analysis

In the proposed model, different degradation modes were considered: fiber breakage in traction as well as in compression, matrix cracking and fiber-matrix debonding. For a 3D case, the strain energy density [14-15] of the damaged ply is defined as follow:

$$e_D = \frac{1}{2} \left( \frac{1}{(1-D_{11})} \left[ \frac{(\sigma_{11})^2}{E_{11}^0} - \left( \frac{\nu_{12}^0}{E_{11}^0} + \frac{\nu_{21}^0}{E_{22}^0} \right) \sigma_{11} \sigma_{22} - \left( \frac{\nu_{13}^0}{E_{11}^0} + \frac{\nu_{31}^0}{E_{33}^0} \right) \sigma_{11} \sigma_{33} - \left( \frac{\nu_{23}^0}{E_{22}^0} + \frac{\nu_{32}^0}{E_{33}^0} \right) \sigma_{22} \sigma_{33} \right] + \frac{\langle -\sigma_{22} \rangle_-^2}{E_{22}^0} + \frac{\langle -\sigma_{33} \rangle_-^2}{E_{33}^0} + \frac{1}{(1-D_{22})} \left[ \frac{\langle \sigma_{22} \rangle_+^2}{E_{22}^0} + \frac{\langle \sigma_{33} \rangle_+^2}{E_{33}^0} \right] + \frac{1}{(1-D_{12})} \left[ \frac{(\sigma_{12})^2}{G_{12}^0} + \frac{(\sigma_{23})^2}{G_{23}^0} + \frac{(\sigma_{31})^2}{G_{31}^0} \right] \right) \quad (1)$$

where  $E_{22}^0 = E_{33}^0$ ,  $G_{12}^0 = G_{13}^0$ ,  $\nu_{12}^0 = \nu_{13}^0$ ,  $G_{23}^0 = E_{33}^0 / (2(1 + \nu_{23}^0))$ .

The symbols  $\langle \bullet \rangle_-$  and  $\langle \bullet \rangle_+$  introduced in equation (1), to model the unilateral effect for the effective transverse stress, mean the negative and positive part of  $\bullet$ , respectively.

From this formula we derive the thermodynamic force vector  $Y$  conjugated to damage, in order to describe the initiation and progression of degradation mechanisms:

$$Y = \frac{\partial \langle \langle e_D(\sigma, d) \rangle \rangle}{\partial d}$$

where the symbol  $\langle \langle \bullet \rangle \rangle$  in equation (2) means the average value of the quantity  $\bullet$  within the thickness.

The activation of damage and its evolution is governed by the square root of a linear combination of the two thermodynamic forces  $Y_{22}$  and  $Y_{12}$ :

$$Y = \sup_{\tau \leq t} \left( \sqrt{Y_{12} + b_1 Y_{22}} \right)$$

where  $b_1$  is a coupling term between the transverse and shear damage. The variables  $Y_{22}$  and  $Y_{12}$  are defined according to Equation (2):

$$Y_{22} = \frac{\partial \langle \langle e_d \rangle \rangle}{\partial D_{22}} = \frac{\langle \sigma_{22} \rangle_+^2}{2(1-D_{22})^2 E_{22}^0} \left( \frac{\langle \sigma_{22} \rangle_+^2}{E_{22}^0} + \frac{\langle \sigma_{33} \rangle_+^2}{E_{33}^0} \right) \quad (4)$$

$$Y_{12} = \frac{\partial \langle \langle e_d \rangle \rangle}{\partial D_{12}} = \frac{1}{2(1-D_{12})^2} \left( \frac{(\sigma_{12})^2}{G_{12}^0} + \frac{(\sigma_{23})^2}{G_{23}^0} + \frac{(\sigma_{13})^2}{G_{13}^0} \right)$$

The transverse and shear damage variables  $d_{22}$  and  $d_{12}$  are defined as:

$$\Rightarrow D_{12} = \begin{cases} \frac{\langle \sqrt{\bar{Y}} - \sqrt{Y_{12}^0} \rangle_+}{\sqrt{Y_{12}^c} - \sqrt{Y_{12}^0}}, & \text{if } D_{12} < 1 \text{ and } Y_{12} < Y_{12}^c \\ 1 & \text{otherwise} \end{cases}$$

$$\Rightarrow D_{22} = \begin{cases} b_2 D_{12}, & \text{if } D_{22} < 1 \text{ and } Y_{22} < Y_{12}^c \\ 1 & \text{otherwise} \end{cases}$$

where  $b_2$  is a coupling term between the transverse and shear damages  $Y_{22}$  and  $Y_{12}$  are the limit strength for damage and the threshold strength for the initiation of damage, respectively. The brittle failure is governed by two critical damage thresholds  $Y_{11}^t$  and  $Y_{11}^c$  for the variable  $Y_{11}$ :

$$Y_{11} = \frac{\partial \langle \langle \epsilon_d \rangle \rangle}{\partial D_{11}} = \frac{1}{2(1-D_{11})^2} \left( \frac{(\sigma_{11})^2}{E_{11}^0} - \sum_{i=1}^2 \sum_{j>i}^3 \left( \frac{v_{ij}^0}{E_i^0} + \frac{v_{ji}^0}{E_j^0} \right) \sigma_{ii} \sigma_{jj} \right) \quad (6)$$

The damage fiber is introduced in the model by considering the Young's modulus  $E_{11}$  as a nonlinear and it depends on stresses  $\sigma_{11}$ :

$$\begin{cases} \text{if } \sigma_{11} > 0 \rightarrow \begin{cases} \text{if } Y_{11} > Y_{11}^t & D_{11} = 1 \\ \text{otherwise} & D_{11} = 0 \end{cases} \\ \text{if } \sigma_{11} < 0 \rightarrow \begin{cases} \text{if } Y_{11} > Y_{11}^c & D_{11} = 1 \\ \text{otherwise} & D_{11} = 0 \end{cases} \end{cases}$$

To limit the maximum damage rate and avoid numerical localization of damage, regularization parameters are introduced [16], and the damage variables are corrected as below:

$$\dot{D}_{ij} = \frac{1}{\tau_c} \left( 1 - e^{-a(D_{ij}^c - D_{ij})} \right)$$

The same material constants,  $\tau_c$  and  $a$ , are taken for the three damage evolution laws.

### 2.2.2. Plastic model

The plastic potential function is defined in 3D condition and it is not depended on stresses  $\sigma_{11}$  in the fiber direction because the fiber behavior is assumed to be elastic brittle under tension or compression:

$$\left\{ F(\bar{\sigma}, \sigma_y) = \sqrt{\tilde{\sigma}_{12}^2 + \tilde{\sigma}_{23}^2 + \tilde{\sigma}_{13}^2 + c^2 [\tilde{\sigma}_{22}^2 + \tilde{\sigma}_{33}^2]} - R_0 + \beta p^\alpha \right.$$

where  $c$  is a coupling parameter,  $R_0$  is the initial yield stress, and the quantities  $\beta$  and  $\alpha$  are the hardening parameters. The effective stresses are defined as follows:

$$\tilde{\sigma}_{12} = \frac{\sigma_{12}}{1-D_{12}}; \tilde{\sigma}_{23} = \frac{\sigma_{23}}{1-D_{12}}; \tilde{\sigma}_{13} = \frac{\sigma_{13}}{1-D_{12}}$$

$$\tilde{\sigma}_{22} = \frac{\langle \sigma_{22} \rangle_+}{1-D_{22}} + \langle \sigma_{22} \rangle_-; \tilde{\sigma}_{33} = \frac{\langle \sigma_{33} \rangle_+}{1-D_{22}} + \langle \sigma_{33} \rangle_-$$

The effective inelastic part of the deformation is defined by the flow rule (or normality rule) as:

$$d\bar{\epsilon}^p = d\lambda \frac{\partial F}{\partial \bar{\sigma}} \text{ and } dp = -d\lambda \frac{\partial F}{\partial \sigma_y} = d\lambda \quad (5)$$

where  $d\lambda$  is a nonnegative plastic consistency parameter (plastic multiplier).

### 2.2.3. Delamination model

This section is focalised on the interlaminar delamination that can be generated during machining operations and causes a failure of the workpiece. The delamination mechanism is characterized by the initiation of micro-cracks at the interface of composite plies, which will grow and cause a failure of the material. This damage is exhibited in the machining, particularly when the two adjacent plies are not oriented in the same direction.

Interply delamination was modelled using cohesive-zone element (CZE) available in the Abaqus/Explicit package. The damage is initiated when a quadratic interaction of a function involving the nominal stress ratio reaches a value of one. This criterion is represented as follows [11]:

$$\left\langle \frac{t_n}{t_n^0} \right\rangle^2 + \left\langle \frac{t_s}{t_s^0} \right\rangle^2 + \left\langle \frac{t_t}{t_t^0} \right\rangle^2 = 1 \quad (7) \quad (12)$$

$t$  is a nominal traction stress vector. The subscripts  $n$ ,  $s$ , and  $t$  represent the normal, first shear, and second shear direction, respectively. The superscript  $^0$  represents the peak value of nominal stress. The symbol  $\langle \rangle$  is a Macaulay bracket and denotes the positive part.

The stresses are coupled to the damage parameter as follows:

$$t_n = (1-d) \bar{t}_n, \quad t_s = (1-d) \bar{t}_s, \quad t_t = (1-d) \bar{t}_t$$

where  $d$  is the damage variable and  $\bar{t}$  represents the stress components (without damage) which are predicted by the elastic traction-separation behavior [18].

The damage evolution is defined by the Benzeggagh–Kenane fracture criterion [19] which is based on the energy dissipated by the damage process:

$$G_n^C + \left( G_s^C - G_n^C \right) \left( \frac{G_s + G_t}{G_n + G_s + G_t} \right)^\eta = G^C \quad (9)$$

$G$  is the fracture energy,  $\eta$  is a material parameter given by [23] and  $C$  represents the critical fracture energy.

## 3. Numerical results

### 3.1. Simulation of the orthogonal cutting (10)

In the following subsections, the obtained numerical results with the elastoplastic models (2D and 3D) are presented for the orthogonal cutting operation using three fiber orientations  $45^\circ$ ,  $90^\circ$  and  $-45^\circ$ . The comparison with the experimental results of Iliescu et al. [9] is also done. Finally, the chips

formation and damage development are discussed.

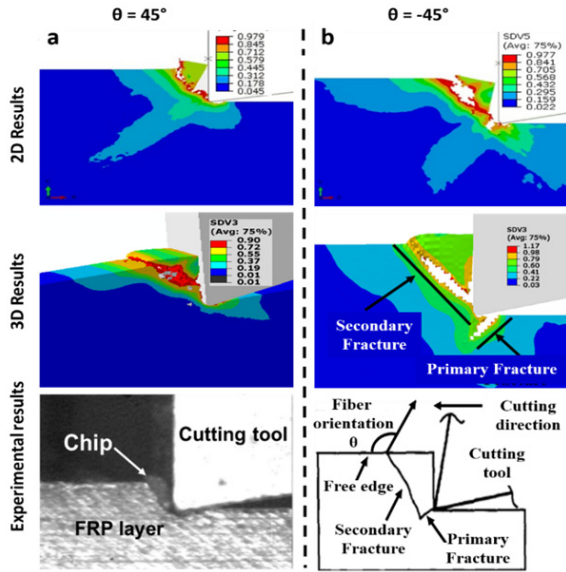


Fig. 2. Chip formation process obtained during FE simulation for different fiber orientations with unidirectional composite compared with experimental results (a)  $\theta = 45^\circ$ ; (b)  $\theta = -45^\circ$

Fig.2 shows the fracture mechanisms observed when machining CFRP composites of 45 and -45 degrees fiber orientation. For 45° fiber orientations, the chip formation mechanism consists of a stretching/crushing of fiber and a shearing at the interface fiber-matrix. The failure occurs at the point of contact of the cutting tool due to compressive crushing-dominated failure. The chip is then formed by fiber-matrix interface shearing to the free surface and ejection of the chip (Fig. 2a). During the cutting of fibers oriented at -45°, the fibers significantly bend and break by pulling out (Fig. 2b).

Fractures, primary and secondary, predicted using the FE model are in good agreement with those observed experimentally by Iliescu [9] (Fig.2a), and Arola and Ramulu [3] (Fig.2b).

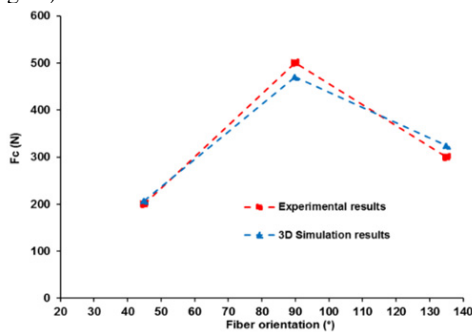


Fig. 3. Cutting force  $F_c$  obtained during FE simulation for different fiber orientations with unidirectional composite compared with experimental results [9] ( $V_c = 60$  m/min,  $a_p = 0.2$  mm,  $\alpha = 0^\circ$ ).

The numerical values of the cutting force  $F_c$  obtained using FE models for different fiber orientations are in good agreement with those obtained experimentally [9] (Fig.3). It

can be noticed that the cutting force is important for a fiber orientation at 90°. This can be explained by the fact that the fibers are firstly crushed and then torn off. During machining of a 90° oriented composite, the wrenching zone located at the point of contact of the tool leads to significant in-depth cracks in the composite.

The conclusion that can be drawn from this graph is that the fiber orientation affects very significantly the cutting forces.

### 3.2. Simulation of the drilling operation

This section shows the numerical results obtained during a conventional drilling operation of CFRP composite laminates. The plates are produced from the stack of unidirectional layers  $[0_4, 90_8, 0_4]$ , which give a total plate thickness of 2 mm. This work interests to thrust forces  $F_t$  and to the interlaminar delamination which occurs between two adjacent layers. The parameters of the used tool are previously mentioned in Section 2.1.

Fig. 4 shows the different stages of a drilling operation with a conventional tool. It also shows the chip morphology obtained in this cutting process. The latter is in the form of powder and this is due to brittle behavior of this type of material.

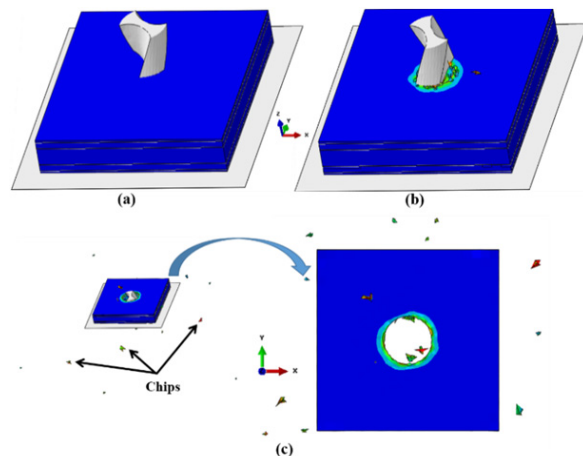


Fig. 4. Steps of hole drilling (a) contact between the tool and the workpiece (b) material removal (c) hole completely drilled.

Fig 5 shows the values of the thrust force  $F_t$  obtained using 3D model for different drill feed rate. It can be noticed that the cutting forces increase when increasing the drill feed rate. The numerical results are in good agreement with those obtained experimentally by Phadnis et al. [10] (Fig.5).

Fig. 6 shows the delamination predicted numerically with the elastoplastic model and experimentally [10] in the input and output of the drilled hole. The conclusion that can be made is that the delamination is more important at the last interface which is located between the two latest layers. These results are in good agreement with those obtained by Phadnis et al. [10] as shown in Fig. 6(a') and Fig. 6(b'). The appearance of this type of delamination is due to the vacuum

which there is under the drilled workpiece and so-called drilling operation, "in the air".

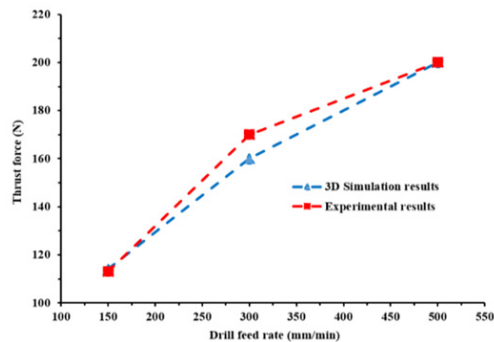


Fig. 5. Comparison between experimental [10] and 3D Simulation thrust forces.

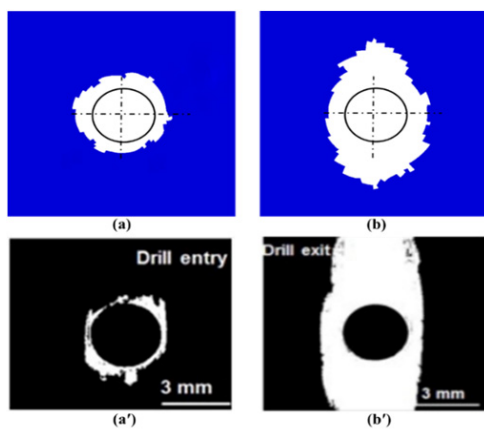


Fig. 6. Drill entry delamination (a) simulation result; (a') experimental result. [10]. Drill exit delamination (b); simulation result (b') experimental result. [10].

#### 4. Conclusion

The main contribution of the current work concerns the development of a complete mechanical approach that integrates coupling between damage and elastic-plastic behaviors to accurately simulate the cutting process of FRP composites. The original point of this work is the consideration of the interply interface using Cohesive Zone Elements (CZE), and prediction of interply damage. The comparison of the obtained results with experiments shows an accurate and realistic prediction of the chip formation process, cutting forces and induced cutting damage. The chip formation process can be clearly described and analyzed by the simulation of the physical mechanisms such as the primary and secondary ruptures. Moreover the proposed model allows to predict accurate cutting forces as shown by the validation with experimental results taken from the literature.

Finally the model allows to study the effect of the drilling parameters on the multi-layers CFRP composites and defines the delamination which can occur at the interply interface. Furthermore, we intend to include the temperature in the finite

element model in order to investigate the thermal effect on the damage initiation and growth. That will be done in future work.

#### References

- [1] Koplev, A. Lystrup, A. Vorm, T. The cutting process, chips and cutting forces in machining CFRP. *Composites* 1983; 14:371–76.
- [2] Wang, D.H. Ramulu, M. Arola, D. Orthogonal cutting mechanisms of graphite/epoxy composite. Part I: Unidirectional Laminate. *Int J Mach Tool Manuf* 1995; 35:1623-1638.
- [3] Arola, D. Ramulu, M. Wang, D.H. Chip formation in orthogonal trimming of graphite/epoxy. *Compos Part A* 1996; 27:121–33.
- [4] Arola, D. and Ramulu, M. Orthogonal cutting of fiber-reinforced composites: a finite element analysis. *Int. J. Mech. Sci.* 1997 39:597-613.
- [5] Venu Gopala Rao, G. Mahajan, P. Bhatnagar, N. Micro-mechanical modelling of machining of FRP composites-cutting force analysis. *Compos. Sci. Technol* 2007; 67:579-93.
- [6] Lasri L. Nouari, M. El-Mansori, M. Modelling of chip separation in machining unidirectional FRP composites by stiffness degradation concept. *Compos. Sci. Technol* 2009; 69: 684-692.
- [7] Santiuste, C. Soldani, X. Miguélez, H.M. Machining FEM model of long fiber composites for aeronautical components, *Compos Struct* 2010; 92: 691-98.
- [8] Zenia S, Ben Ayed L, Nouari M, Delamézière A. Numerical prediction of the chip formation process and induced damage during the machining of carbon/epoxy composites. *Int J Mech Sci* 2015; 90: 89-101.
- [9] Iliescu, D. Gehin, D. Iordanoff, I. Giro, F. Gutiérrez, M.E. A discrete element method for the simulation of CFRP cutting. *Compos. Sci. Technol* 2010; 70:73-80.
- [10] Phadnis VA, Makhadmeh F, Roy A, Silberschmidt VV. Drilling in carbon/epoxy composites: Experimental investigations and finite element implementation. *Compos Part A* 2013, 47: 41-51.
- [11] ABAQUS Documentation for version 6.11-2 Dassault systems Simulia, 2011.
- [12] Feld N. Vers un pont micro-méso de la rupture en compression des composites stratifiés. PhD thesis; pp 115, 2011.
- [13] Shin DK, Kim HC, Lee JJ. Numerical analysis of the damage behavior of an aluminum/CFRP hybrid beam under three point bending *Compos: Part B* 2014; 56:397–407.
- [14] Ladeveze, P. and LeDantec, E. Damage modelling of the elementary ply for laminated composites. *Compos Sci Technol* 1992; 43: 257-67.
- [15] Lubineau, G. and Ladevèze, P. Construction of a micromechanics-based intralaminar mesomodel, and illustrations in ABAQUS/Standard. *Comput. Mater. Sci* 2008; 43:137-45.
- [16] Allix, O. Feissel, P. Thévenet, P. A delay damage mesomodel of laminates under dynamic loading basic aspects and identification issues. *Comput Struct* 2003; 81:1177–1191.
- [17] Lemaitre, J. and Chaboche, J.L. *Mechanics of Solid Materials*, Cambridge University Press, Cambridge, UK 1990.
- [18] Turon A, Dávila CG, Camanho PP, Costa J. An engineering solution for mesh size effects in the simulation of delamination using cohesive zone models. *Eng Fract Mech* 2007;74(10):1665–82.
- [19] Benzeggagh M, Kenane M. Measurement of Mixed-Mode Delamination Fracture Toughness of Unidirectional Glass/Epoxy Composites with Mixed-Mode Bending Apparatus. *Compos Sci Technol* 1996; 56: 439–49.